



Porous Se@SiO₂ nanocomposites play a potential inhibition role in hyperoxaluria associated kidney stone by exerting antioxidant effects

Chen Ye^{1#}, Lin Zhao^{1#}, Jiaying Miao^{1#}, Chengyu Gong², Yuanguai Chen¹, Shengfei Qin³, Nicholas N. Tadros⁴, Stefan Aufderklamm⁵, Wenli Jiang^{2*}, Guoying Deng^{6*}, Shaoxiong Ming^{1*}

¹Department of Urology, Shanghai Changhai Hospital, Naval Medical University, Shanghai, China; ²Department of Biochemistry and Molecular Biology, College of Basic Medical Sciences, Naval Medical University, Shanghai, China; ³Department of Urology, Shanghai Fourth People's Hospital, School of Medicine, Tongji University, Shanghai, China; ⁴Division of Urology, Southern Illinois University, Springfield, IL, USA; ⁵Department of Urology, Eberhard-Karls University Tübingen, Tübingen, Germany; ⁶Trauma Center, Shanghai General Hospital, Shanghai Jiao Tong University School of Medicine, Shanghai, China

Contributions: (I) Conception and design: S Ming, C Ye; (II) Administrative support: G Deng, W Jiang; (III) Provision of study materials or patients: L Zhao, J Miao; (IV) Collection and assembly of data: C Gong, Y Chen; (V) Data analysis and interpretation: S Qin; (VI) Manuscript writing: All authors; (VII) Final approval of manuscript: All authors.

[#]These authors contributed equally to this work as co-first authors.

^{*}These authors contributed equally to this work as co-corresponding authors.

Correspondence to: Wenli Jiang, PhD. Department of Biochemistry and Molecular Biology, College of Basic Medical Sciences, Naval Medical University, No. 800, Xiangyin Road, Shanghai 200433, China. Email: jwlsally@163.com; Guoying Deng, MD, PhD. Trauma Center, Shanghai General Hospital, Shanghai Jiao Tong University School of Medicine, No. 650, New Songjiang Road, Shanghai 201620, China. Email: guoying.deng@shgh.cn; Shaoxiong Ming, MD. Department of Urology, Shanghai Changhai Hospital, Naval Medical University, No. 800, Xiangyin Road, Shanghai 200433, China. Email: sxmingnk@foxmail.com.

Background: Nephrolithiasis seriously affects people's health with increasing prevalence and high recurrence rates. However, there is still a lack of effective interventions for the clinical prevention of kidney stones. Hyperoxaluria-induced renal tubular epithelial cell (TEC) injury is a known key factor in kidney stone formation. Thus, developing new drugs to inhibit the hyperoxaluria-induced TEC injury may be the best way.

Methods: We synthesized the Se@SiO₂ nanocomposites as described in Zhu's study. The size and morphology of the Se@SiO₂ nanocomposites were captured by transmission electron microscopy. Cell viability was measured by a Cell Counting Kit-8 (CCK-8) assay. The mice were randomly divided into the following four groups: (I) the control group (n=6); (II) the Se@SiO₂ group (n=6); (III) the glyoxylic acid monohydrate (GAM) group; and (IV) the GAM + Se@SiO₂ group (n=6). The concentration of Se in the mice was quantified using inductively coupled plasma atomic emission spectroscopy.

Results: The CCK-8 assays showed that Se@SiO₂ nanocomposites had almost no obvious cytotoxicity on the Transformed C3H Mouse Kidney-1 (TCMK-1) cell. The mice kidney Se concentration levels in the Se@SiO₂ groups (Se@SiO₂ 6.905±0.074 mg/kg; GAM + Se@SiO₂ 7.673±2.85 mg/kg) (n=6) were significantly higher than those in the control group (Control 0.727±0.072 mg/kg; GAM 0.747±0.074 mg/kg) (n=6). The Se@SiO₂ nanocomposites reduced kidney injury, calcium oxalate crystal deposition, and the osteoblastic-associated proteins in the hyperoxaluria mice models.

Conclusions: Se@SiO₂ nanocomposites appear to protect renal TECs from hyperoxaluria by reducing reactive oxygen species production, suggesting the potential role of preventing kidney stone formation and recurrence.

Keywords: Se@SiO₂ nanocomposites (Se@SiO₂ NPs); hyperoxaluria; kidney stone; antioxidant

Submitted Oct 10, 2023. Accepted for publication Mar 06, 2024. Published online Apr 18, 2024.

doi: 10.21037/tau-23-511

View this article at: <https://dx.doi.org/10.21037/tau-23-511>

Introduction

Nephrolithiasis is a common urological disease with increasing prevalence worldwide (1,2). If left untreated, kidney stones may lead to different levels of hematuria, urinary infection, and urinary obstruction, which in turn may cause permanent renal function impairment. With the development of endoscopic laser lithotripsy and extracorporeal shock-wave lithotripsy, the treatment of urinary stones has become less invasive and more efficient (3-5). Due to the high recurrence rate (nearly 50% within 5 years of the first occurrence), nephrolithiasis patients suffer from recurrent pain, which leads to increased hospitalization and thus increased medical costs (6-8). It is widely reported that nearly 80% of kidney stones are composed of calcium, especially calcium oxalate (CaOx) (9,10); however, there is still a lack of effective interventions for the clinical prevention of kidney stones.

Hyperoxaluria-induced renal tubular epithelial cell (TEC) injury is an important factor in kidney stone formation (11). Oxidative stress with increasing reactive oxygen species (ROS) is thought to be a significant mechanism underlying the cytotoxicity of high concentrations of oxalate in TECs (12,13). Thus, agents with antioxidant properties might suppress kidney stone formation.

Selenium (Se), which is an essential minor element in the human body with multiple biological functions, is known

to have excellent antioxidant properties (14). However, the margin between the safety and toxicity of Se is narrow. The development of cardiac and pulmonary symptoms in cases of severe toxicity can ultimately result in mortality (15). The development of nanotechnology in recent years has promoted the progress of drug research (16). Taking advantage of nanotechnology, the release of Se can be well controlled *in vivo*. In previous research, we developed Se@SiO₂ nanocomposites (NPs) that have good antioxidant properties and biosafety in the disease process of steroid-induced osteonecrosis and acute lung injury (17,18). We hypothesized that Se@SiO₂ NPs might protect TECs from hyperoxaluria by reducing ROS production.

In this study, we investigated whether Se@SiO₂ NPs ameliorated hyperoxaluria-induced kidney stone formation in mice models. The potential mechanisms underlying the protective effect of Se@SiO₂ NPs on hyperoxaluria-induced renal TEC injury were also explored. The results of this study may provide a new direction for the treatment of kidney stones. We present this article in accordance with the ARRIVE reporting checklist (available at <https://tau.amegroups.com/article/view/10.21037/tau-23-511/rc>).

Methods

Synthesis of Se@SiO₂ NPs

We synthesized the Se@SiO₂ NPs as described previously (17,18). First, a mixture of 39.5 mg of Se powder and 5 mL of oleic acid (OA) were stirred continuously for 30 min at 120 °C in a nitrogen atmosphere. Second, the Se-OA precursor was formed after the mixture was heated to 220 °C. Next, a mixture of oleylamine (OAM; 5 mL), OA (5 mL), and cuprous chloride (CuCl) (49.5 mg) was heated to 120 °C to remove any moisture. Subsequently, the mixture was heated to 220 °C, and the above Se-OA precursor was quickly injected into the mixture. The solution was incubated at 220 °C for 5 min. For the synthesis, the Cu_{2-x}Se nanocrystals were washed with ethanol and dispersed in normal hexane. Subsequently, the Cu_{2-x}Se solution (3 mL), n-hexanol (30 mL), Triton X-100 (3 mL), and deionized water (0.9 mL) were stirred for 30 min, and tetraethyl orthosilicate (0.15 mL) and ammonia

Highlight box

Key findings

- The Se@SiO₂ nanocomposites (NPs) may decrease hyperoxaluria-induced kidney damage and kidney stone formation via their antioxidant benefits.

What is known and what is new?

- Hyperoxaluria-induced renal tubular epithelial cell injury is a key factor in kidney stone formation.
- The Se@SiO₂ NPs may decrease hyperoxaluria-induced kidney damage.

What is the implication, and what should change now?

- Se@SiO₂ NPs might be a potential drug for the treatment of nephrolithiasis. Further studies are warranted to validate its applicability in humans.

(0.20 mL) were then successively added under rapid stirring. The solid Se@SiO₂ NPs were formed by centrifugation after stirring for 24 h. To obtain the porous Se@SiO₂ NPs for the release of Se, the solid Se@SiO₂ NPs were dispersed in 20 mL of polyvinylpyrrolidone (PVP) aqueous solution (10 mg/mL) and heated to 95 °C for 2 h under very slow stirring.

Transmission electron microscopy (TEM)

The size and morphology of the Se@SiO₂ NPs were captured by TEM using a JEM-2100F microscope (JEOL, Tokyo, Japan). X-ray diffraction (XRD) was measured by a D/max-2550 PCX-ray diffractometer (Rigaku, Tokyo, Japan).

In-vitro safety of Se@SiO₂ NPs

The mouse kidney TECs (TCMK-1) were plated in 96-well plates (1×10⁴ cells/well) and incubated overnight before undergoing overnight treatments with different concentrations of NPs. After being incubated for 24 h, cell viability was measured using a Cell Counting Kit-8 (CCK-8) (Dojindo, Kyushu Island, Japan) with an ELx800 plate reader (BioTek, Winooski, VT, USA).

Animal experimental design

The study was approved by the Animal Care and Use Committee of Shanghai Changhai Hospital (hospital project license, No. 2020QH08). All the animals were kept under specific pathogen-free conditions, in compliance with Guide for the Care and Use of Laboratory Animals (Eighth Edition). A protocol was prepared before the study without registration. In total, 24 C57BL/6 male mice (aged 8 weeks old and weighing 20±1 g) were purchased from Shanghai SLAC Laboratory Animal Co., Ltd. The mice were randomly divided into the following 4 groups: (I) the control group (n=6), which was intraperitoneally injected with normal saline/day; (II) the Se@SiO₂ group (n=6), which was intraperitoneally injected with Se@SiO₂ (1 mg/kg/day); (III) the glyoxylic acid monohydrate (GAM) group (i.e., the nephrolithiasis group), which was intraperitoneally injected with GAM (100 mg/kg/day) for 7 days consecutively; and (IV) the GAM + Se@SiO₂ group, which was intraperitoneally injected with GAM (100 mg/kg/day) after 8 h of Se@SiO₂ (1 mg/kg/day) pre-treatment. At the end of the experimental procedures, all

the mice were euthanized. Serum samples and urine samples were collected and stored at -80 °C. Left renal samples were collected and fixed with 4% polyformaldehyde (PFA). Right renal samples were collected and stored in liquid nitrogen.

Basic body characteristics and urinary oxalate and Se quantitative analysis

The body weight of the mice was measured. Urinary oxalate excretion levels were determined using an oxalate assay kit (Sigma, MAK179; St. Louis, MO, USA). The standard curves and samples were prepared and measured according to the instructions. After the treatment of the part renal tissues with aqua regia, the mixed solutions were filtered. The concentration of Se was measured by inductively coupled plasma atomic emission spectroscopy as previously described (17,18).

Histology examination analysis

The left renal samples were fixed in 4% PFA, embedded with paraffin, and serially sectioned at 6-µm thickness for staining. Hematoxylin and eosin (H&E) staining was performed to conduct the histology examination and assess the renal injury level. We then evaluated 10 non-continuous fields from the cortex of each section (400× and 200× magnification).

TUNEL analysis

Apoptosis was detected using a TUNEL apoptosis assay kit (Beyotime, Shanghai, China). The whole process was performed in accordance with the manufacturer's instructions, and the samples were observed under a fluorescence microscope before anti-fluorescence quenching.

ROS activity analysis

The ROS levels of the kidney tissues were measured using the dihydroethidium in accordance with the manufacturer's instructions. The tissues were incubated with dihydroethidium staining solution for 30 min at 37 °C. The tissues were then washed with phosphate buffered saline (PBS) in the dark and incubated with 4',6-diamidino-2-phenylindole staining solution for 10 min. The tissues were then washed with PBS in the dark. Fluorescence images were captured using a Panoramic MIDI (3DHISTECH), and ROS production was measured using ImageJ software.

The intracellular ROS levels were measured using the Carboxy-H2DFFDA kit in accordance with the manufacturer's protocol. The TCMK-1 cells were plated in a 6-well plate at 10^6 cells/well with an oxalate (0.5 mM) or Se@SiO₂ (90 µg/mL) treatment for 3 h, then washed with PBS and incubated with carboxy-H2DCFDA staining solution for 1.5 h at 37 °C. The cells were subsequently rinsed with PBS under low light conditions. Fluorescent images were acquired utilizing a Cytation 5 Cell Imaging Multi-Mode Reader (BioTek), and quantification of ROS generation was performed using ImageJ software.

Quantitative real-time polymerase chain reaction (qRT-PCR)

The RNA was isolated from the tissues using the RNeasy Mini kit (Qiagen, Dusseldorf, Germany) following the manufacturer's instructions. Complementary DNA synthesis was performed using a PrimeScript RT Master Mix Kit (Takara Bio, Dalian, China). QRT-PCR analysis was conducted on an ABI PRISM[®] 7500 system (Thermo Fisher Scientific, Waltham, MA, USA) using SYBR Premix Ex Taq[™] II, specific forward and reverse primers, and double distilled water. The cycling conditions consisted of an initial denaturation step at 95 °C for 5 min followed by 42 cycles of denaturation at 95 °C for 10 s, annealing at 60 °C for 20 s, extension at 72 °C for 20 s, and a final extension step at 72 °C for 20 s. The primers were as follows: bone morphogenetic protein 2 (BMP-2; Forward: 5'-CCTATATGCTCGACCTGTACCG-3'; Reverse: 5'-CTGGCTGTGGCAGGCTTTAT-3'), osteopontin (OPN; Forward: 5'-CTCGAAGACTCTGATGATGT-3'; Reverse: 5'-TGTCAGGTCTGCGAACTTCT-3'), and glyceraldehyde-3-phosphate dehydrogenase (GAPDH) (Forward: 5'-ACCCAGAAGACTGTGGATGG-3'; Reverse: 5'-CACATTGGGGGTAGGAACAC-3'). The expression of the target genes was normalized to GAPDH levels. All the assays were repeated 3 times. Gene expression was calculated with $2^{-\Delta\Delta CT}$.

Maleic dialdehyde (MDA) and superoxide dismutase (SOD) assays

We took part of the kidney tissue, rinsed it in normal saline, sucked it dry with filter paper, weighed it, added normal saline 9 times the weight of the kidney tissue, homogenized

it for 5 min, centrifuged it for 10 min at 3,000 r/min, and sucked it up with a micropipette. The absorbance values of SOD and MDA were detected at 550 and 532 nm by ultraviolet-visible (UV-Vis) spectrophotometry according to the operation requirements of the SOD and MDA kit.

Cell apoptosis assay

The cell apoptosis analysis kit was utilized to assess cell apoptosis. TCMK-1 cells were trypsinized, PBS-washed, and then resuspended in 1 × Annexin-binding buffer. Early apoptosis was identified by staining with Alexa Fluor[®] 488 Annexin V (Thermo Fisher Scientific) and propidium iodide (PI). The stained cells were analyzed using a CytoFLEX flow cytometer from Beckman Coulter Inc. (Brea, CA, USA). Data acquisition was performed using Cell Quest software (version 3.0).

Statistical analysis

The data analysis was performed using GraphPad Prism 7 (GraphPad Software Inc., San Diego, CA, USA). The data are expressed as the mean ± standard deviation. The unpaired Student's *t*-test and a one-way analysis of variance were used for the comparisons. P values <0.05 were considered significant.

Results

The characterization of porous Se@SiO₂ NPs

We prepared the porous Se@SiO₂ NPs as previously described (17,18). The XRD pattern showed an increase in the low angle region of the solid Se@SiO₂ NPs due to the silica coating (Figure 1A). According to the standard Se phase (Joint Committee on Powder Diffraction Standards, JCPDS card No. 65-1876), the distinctive peaks of the solid Se@SiO₂ NPs had a hexagonal shape (Figure 1A). The morphology and size of the Se@SiO₂ NPs were also observed by TEM (Figure 1B-1D). The diameters of the solid Se@SiO₂ NPs were about 55 nm. Many small (size <5 nm) and irregular Se quantum dots were interspersed from the center to the surface of the NPs. After the hot PVP solution treatment, the Se@SiO₂ NPs showed a porous structure (Figure 1D), which is facile for the release of Se. The CCK-8 assays showed that the Se@SiO₂ NPs had almost no obvious cytotoxicity in the TCMK-1 (Figure 1E).

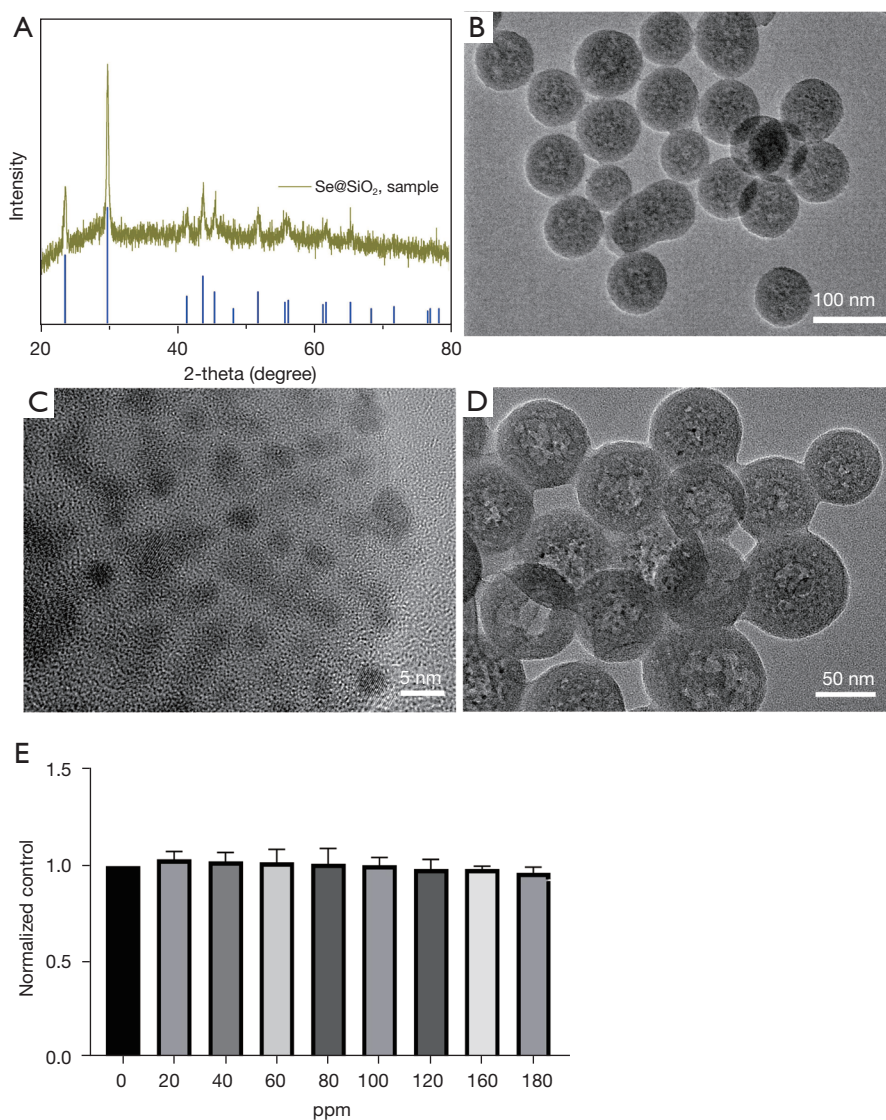


Figure 1 Characterization of the porous Se@SiO₂ nanocomposites. (A) XRD pattern of the porous Se@SiO₂ nanocomposites and standard Se phase (JCPDS and No. 65-1876). (B) TEM of the porous Se@SiO₂ nanocomposites. (C,D) Low-magnified and medium-magnified images of the porous Se@SiO₂ nanocomposites. (E) The cell viability of the TCMK-1 cells treated with different concentrations of the porous Se@SiO₂ nanocomposites for 24 h. XRD, X-ray diffraction; TEM, transmission electron microscopy; ppm, parts per million.

General results of the hyperoxaluria mouse model following the porous Se@SiO₂ nanocomposite treatment

The schematic protocol for the animal experiment in our study is shown in *Figure 2A*. There were no significant differences in the body weight of the mice in the control, Se@SiO₂, GAM, and GAM + Se@SiO₂ groups (*Figure 2B*). The urinary oxalate excretion levels differ significantly among the GAM and GAM + Se@SiO₂ groups, (*Figure 2C*). The mice kidney Se concentration levels of the Se@SiO₂

and GAM + Se@SiO₂ groups were significantly higher than those of the control and GAM groups (*Figure 2D*).

The porous Se@SiO₂ NPs reduced kidney injury, CaOx crystal deposition, and osteoblastic-associated proteins in the hyperoxaluria mouse model.

The H&E staining showed significant kidney histological injuries at the junction of the medullary and cortex in the GAM group, but these injuries were significantly ameliorated in the GAM + Se@SiO₂ group (*Figure 3A*, left).

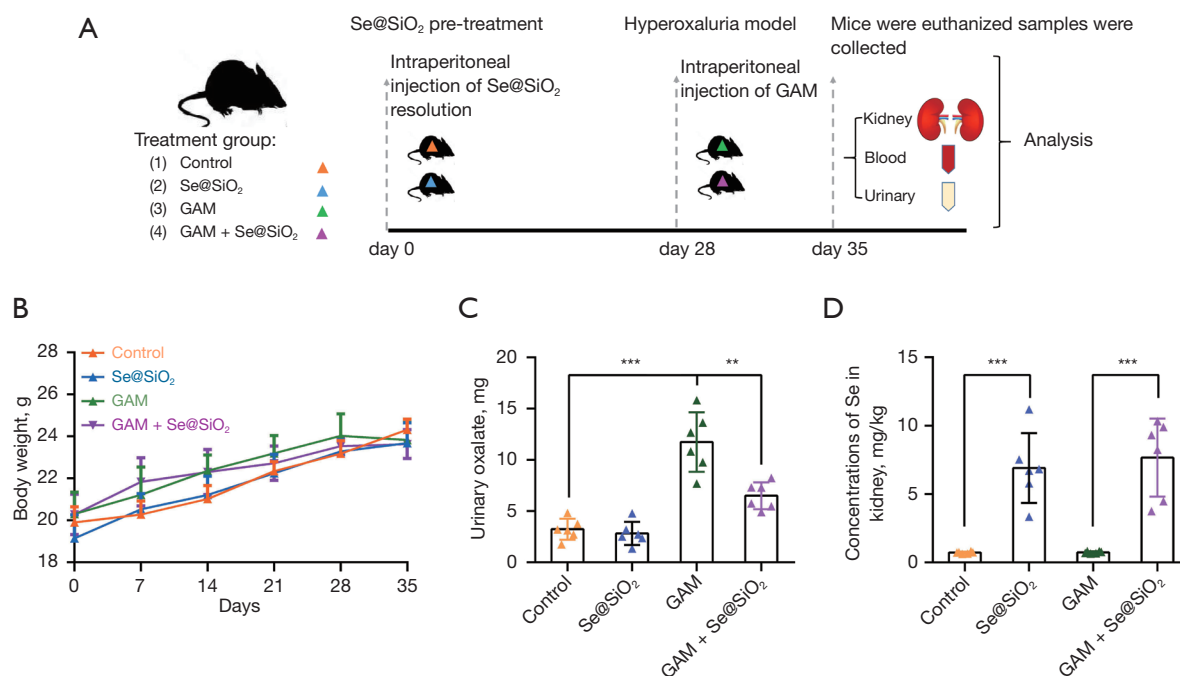


Figure 2 General results of the hyperoxaluria mouse model treated with porous Se@SiO₂ nanocomposites. (A) The schematic protocol of the animal experiment. (B) The body weight curves of the mice. (C) The urinary oxalate excretion levels of the mice. (D) The mice kidney Se concentration levels. **, P<0.01; ***, P<0.001. GAM, glyoxylic acid monohydrate.

Von Kossa staining revealed that the CaOx crystal deposition mass was higher in the GAM group than in the control group. Following the porous Se@SiO₂ treatment, the CaOx crystal deposition mass was significantly lower in the GAM + Se@SiO₂ group than in the GAM group (Figure 3A, right). The levels of Scr and blood urea nitrogen (BUN) were lower in the GAM + Se@SiO₂ group than in the GAM group (Figure 3B). We further detected the expression of the osteogenic proteins OPN and bone morphogenetic protein 2 (BMP2), which are closely related to the formation of CaOx nephrolithiasis in the mice kidney tissues (19). The qRT-PCR assays showed that the level of OPN and BMP2 in the mice kidney tissues was much lower in the GAM + Se@SiO₂ group than in the GAM group (Figure 3C).

Porous Se@SiO₂ NPs reduced oxidative stress and apoptosis both *in vivo* and *in vitro*

We detected the ROS levels in the mice kidney tissues after the GAM treatment. Compared to the control group, GAM significantly increased the ROS levels. However, ROS production was significantly decreased in the GAM +

Se@SiO₂ group (Figure 4A). We then measured the levels of MDA and SOD, which are biomarkers of oxidative stress, in the kidney tissues of the mouse model using the MDA and SOD assay kits. The results showed that GAM significantly increased the level of MDA and decreased the activity of SOD. However, the porous Se@SiO₂ NPs significantly decreased the level of MDA and increased the activity of SOD in the GAM + Se@SiO₂ group (Figure 4B). Further, the TUNEL assays showed that the positive rate of apoptosis was markedly increased in the GAM group, while the apoptotic level of the kidney tissue was significantly decreased in the GAM + Se@SiO₂ group (Figure 4C). We also conducted fluorescent dichlorofluorescein (DCF) assays and flow cytometry in the TCMK-1 cells after the oxalate treatment. The *in vitro* results were consistent with the *in vivo* results (Figure 4D, 4E).

Discussion

The incidence of urolithiasis depends on several factors like geography, ethnicity, diet or genetics. The prevalence of urinary stone development varies from 4% to 20% (20). Several countries like the United States of America showed

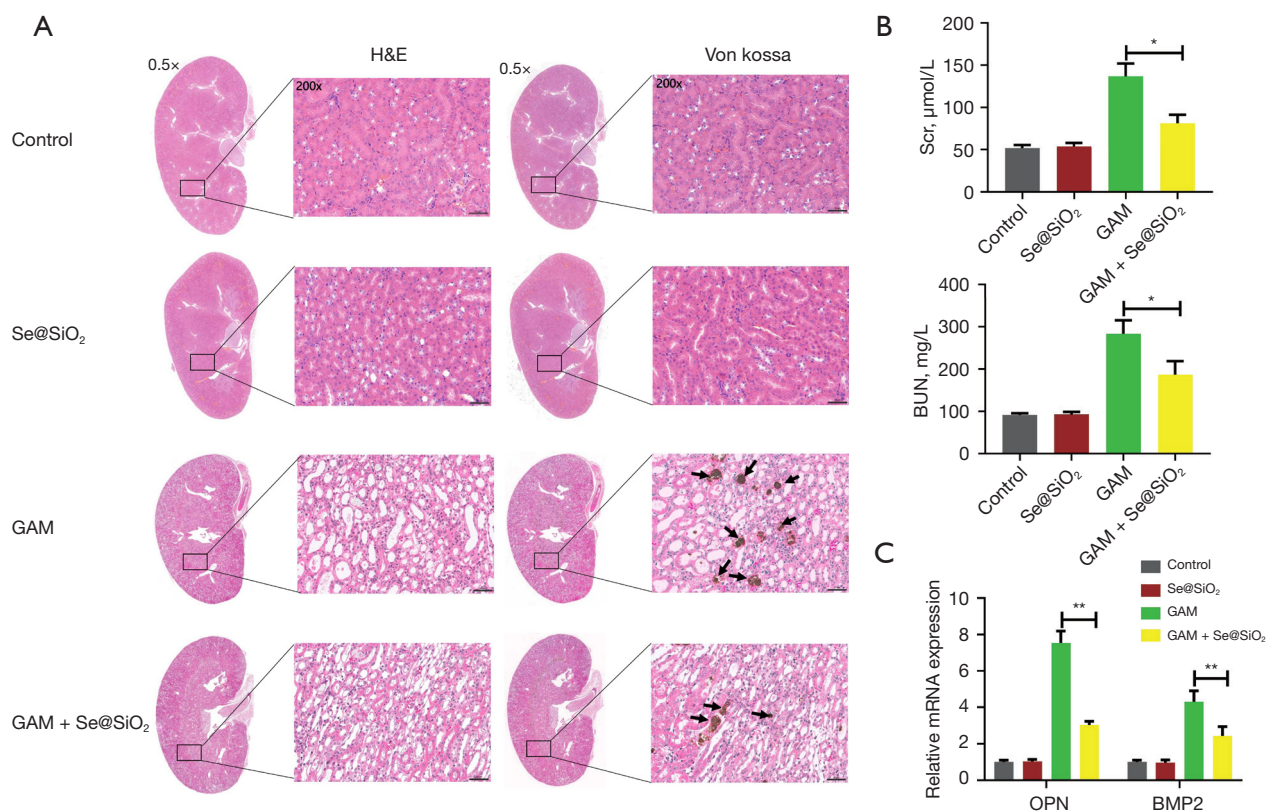


Figure 3 Porous Se@SiO₂ nanocomposites inhibit hyperoxaluria-induced CaOx crystal deposition and function impairment on renal. (A) H&E staining (left, magnification $\times 0.5$ for full view, magnification $\times 200$ for local zoom) and Von Kossa staining (right, magnification $\times 0.5$ for full view, magnification $\times 200$ for local zoom) of the mice kidney tissues. The arrows point to CaOx crystal deposition mass. Scale bar: 50 μm . (B) The levels of Scr and BUN in the serum of the mice. (C) The RNA expression level of OPN and BMP2 in the kidney tissues of the mice. *, $P < 0.05$; **, $P < 0.01$. H&E, Hematoxylin and eosin; GAM, glyoxylic acid monohydrate; BUN, blood urea nitrogen; OPN, osteopontin; BMP2, bone morphogenetic protein 2.

an increased prevalence of kidney stones, which is likely due to unhealthy lifestyle habits, such as high-protein/high-sugar/high-salt diets, smoking, drinking, and less physical activity/obesity (21–23). However, while these unfavorable factors might elevate the concentrations of oxalate, calcium, and uric acid in the urine, kidney stone formation is not a simple physicochemical disorder.

The majority of research suggests that stone formation is a form of pathological biomineralization or ectopic calcification, involving epithelial to mesenchymal transition, epithelial to osteoblast transformation, and the remodeling of the extracellular matrix in nephrons, especially in TECs (24–26). Notably, ROS-associated oxidative stress-induced TEC injury and inflammation have been considered the initial triggers of kidney stone formation (27,28). It is also well established that oxidative stress-induced injury is

involved in the pathogenesis of a variety of chronic diseases, such as cardiovascular and cerebrovascular diseases, neurodegenerative diseases, and diabetes (27,29–31). Thus, these diseases are risk factors for nephrolithiasis (32,33). Further, numerous clinical and experimental studies have confirmed that antioxidant treatments are effective in the therapy of these diseases, including nephrolithiasis (34–37).

Selenium is a recognized health-benefiting element that could play an important role in protecting cells against oxidative stress injury (14). Our previous studies showed that our Se@SiO₂ NPs protect cells from chemotherapy-induced oxidative stress injury by attenuating doxorubicin-induced cardiotoxicity and attenuating cisplatin-induced acute kidney injury (38,39). Due to the controllable release of Se, our porous Se@SiO₂ NPs have good biosafety *in vivo*. In this study, the CCK-8 assays first showed that the

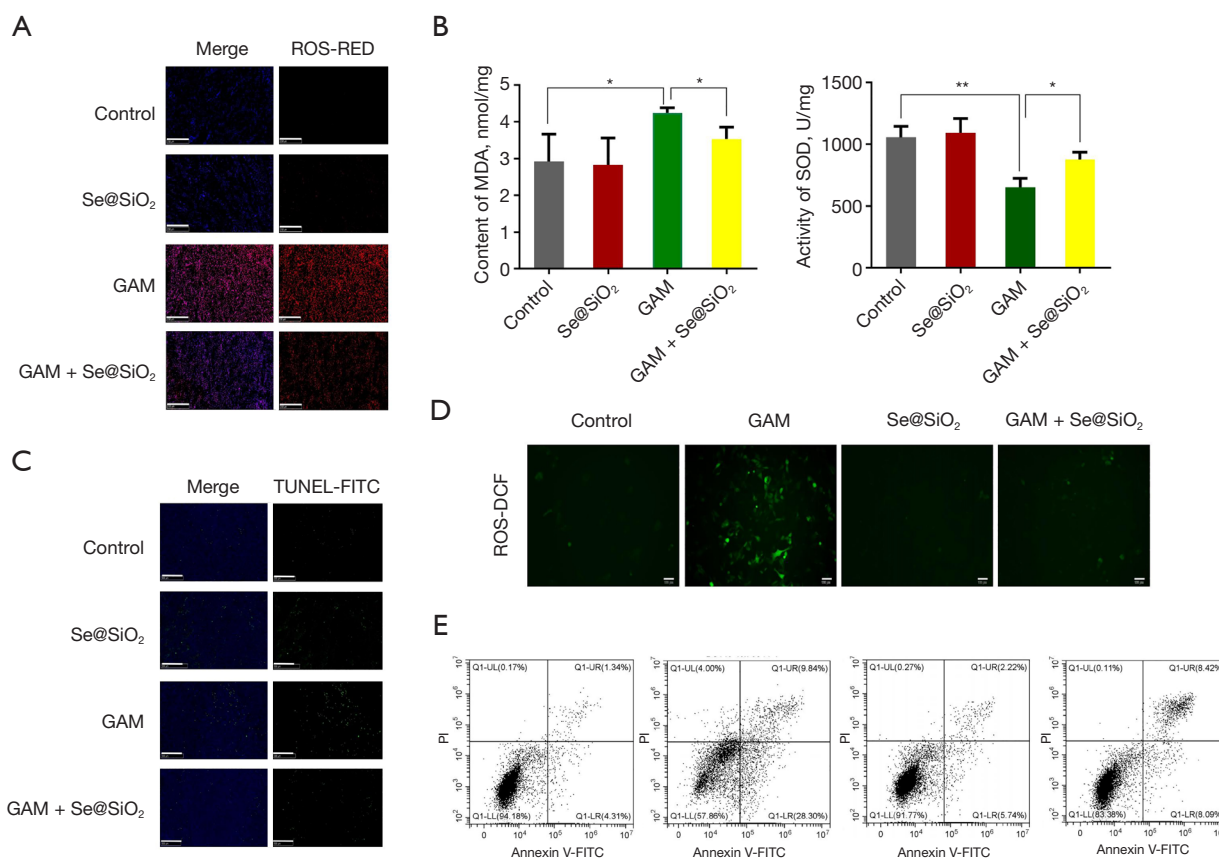


Figure 4 Porous Se@SiO₂ nanocomposites reduced oxidative stress and apoptosis. (A,C) Representative images of ROS and TUNEL assays in mice kidney tissues observed under a fluorescence microscope. Scale bar: 250 μ m in A, 500 μ m in C. (B) The levels of MDA and SOD in the mice kidney tissues. (D) Representative images of ROS assays in the TCMK-1 cells observed under a fluorescence microscope. (E) Apoptosis was detected by an Annexin V-FITC + PI kit and the cell apoptosis rate (%). *, $P < 0.05$; **, $P < 0.01$. ROS, reactive oxygen species; GAM, glyoxylic acid monohydrate; MDA, maleic dialdehyde; SOD, superoxide dismutase; FITC, fluorescein isothiocyanate; PI, propidium iodide; DCF, dichlorofluorescein.

Se@SiO₂ NPs had almost no cytotoxicity on the mouse kidney TECs *in vitro*. In the hyperoxaluria mouse model, our results showed that there were no significant differences in the body weight of the mice in the control, GAM, and GAM + Se@SiO₂ groups. The levels of mice kidney Se concentration in the Se@SiO₂ and GAM + Se@SiO₂ groups were significantly higher than those of the control and GAM groups. Further, the H&E and Von Kossa staining showed that the Se@SiO₂ NPs significantly reduced renal injuries and CaOx crystal deposition in the hyperoxaluria mouse model.

Previous studies have indicated that upregulated expressions of BMP2 and OPN are involved in kidney stone formation during excess ROS-induced kidney injury and

inflammation (40,41). In this study, the qRT-PCR assays showed that the levels of OPN and BMP2 in the mice kidney tissues were much lower in the GAM + Se@SiO₂ group than in the GAM group. A study has introduced that high oxalate and CaOx crystals induced the TECs to generate excess ROS, which severely damages cell structure and function through oxidation reactions with lipids, carbohydrates, proteins, and nucleic acids (27). It is well-known that the cells are equipped with mechanisms to decrease ROS availability, such as SOD. In this study, the DCF assay results showed that hyperoxaluria increased the ROS level dramatically, while the Se@SiO₂ NPs significantly inhibited the production of ROS induced by hyperoxaluria in the kidney tissue of the mouse model. The

enzyme-linked immunoassays showed that the Se@SiO₂ NPs significantly reversed the increased level of MDA and the decreased activity of SOD induced by hyperoxaluria. Further, the TUNEL assays showed that the apoptotic level of the kidney tissue was significantly more decreased in the GAM + Se@SiO₂ group than in the GAM group. *In vitro*, the DCF assays and flow cytometry assays also showed that the Se@SiO₂ NPs alleviated the ROS level and cell apoptosis induced by oxalate.

Conclusions

In summary, the Se@SiO₂ NPs may decrease hyperoxaluria-induced kidney damage and kidney stone formation via their antioxidant benefits. Thus, Se@SiO₂ NPs might be a potential drug for the treatment of nephrolithiasis. Further studies are warranted to validate its applicability in humans.

Acknowledgments

Funding: The study was supported by Fund of Shanghai Hongkou District Health Committee (hong wei 2022-29).

Footnote

Reporting Checklist: The authors have completed the ARRIVE reporting checklist. Available at <https://tau.amegroups.com/article/view/10.21037/tau-23-511/rc>

Data Sharing Statement: Available at <https://tau.amegroups.com/article/view/10.21037/tau-23-511/dss>

Peer Review File: Available at <https://tau.amegroups.com/article/view/10.21037/tau-23-511/prf>

Conflicts of Interest: All authors have completed the ICMJE uniform disclosure form (available at <https://tau.amegroups.com/article/view/10.21037/tau-23-511/coif>). The authors have no conflicts of interest to declare.

Ethical Statement: The authors are accountable for all aspects of the work in ensuring that questions related to the accuracy or integrity of any part of the work are appropriately investigated and resolved. The study was approved by the Animal Care and Use Committee of Shanghai Changhai Hospital (hospital project license, No. 2020QH08). All the animals were kept under specific

pathogen-free conditions, in compliance with Guide for the Care and Use of Laboratory Animals (Eighth Edition). A protocol was prepared before the study without registration.

Open Access Statement: This is an Open Access article distributed in accordance with the Creative Commons Attribution-NonCommercial-NoDerivs 4.0 International License (CC BY-NC-ND 4.0), which permits the non-commercial replication and distribution of the article with the strict proviso that no changes or edits are made and the original work is properly cited (including links to both the formal publication through the relevant DOI and the license). See: <https://creativecommons.org/licenses/by-nc-nd/4.0/>.

References

1. Fontenelle LF, Sarti TD. Kidney Stones: Treatment and Prevention. *Am Fam Physician* 2019;99:490-6.
2. Wang K, Ge J, Han W, et al. Risk factors for kidney stone disease recurrence: a comprehensive meta-analysis. *BMC Urol* 2022;22:62.
3. Alexander B, Fishman AI, Grasso M. Ureterscopy and laser lithotripsy: technologic advancements. *World J Urol* 2015;33:247-56.
4. Pavlov VN, Alekseev AV, Pushkarev AM, et al. Extracorporeal shock wave lithotripsy: benefits, limitations and prospects. *Urologia* 2016;(4):122-6.
5. Zou B, Zhou Y, He Z, et al. A critical appraisal of urolithiasis clinical practice guidelines using the AGREE II instrument. *Transl Androl Urol* 2023;12:977-88.
6. Rule AD, Lieske JC, Pais VM Jr. Management of Kidney Stones in 2020. *JAMA* 2020;323:1961-2.
7. Khan SR, Pearle MS, Robertson WG, et al. Kidney stones. *Nat Rev Dis Primers* 2016;2:16008.
8. Chen X, Li S, Shi C, et al. Risk factors and predictors of urogenous sepsis after percutaneous nephrolithotomy for idiopathic calcium oxalate nephrolithiasis. *Transl Androl Urol* 2023;12:1002-15.
9. Spivacow FR, Del Valle EE, Lores E, et al. Kidney stones: Composition, frequency and relation to metabolic diagnosis. *Medicina (B Aires)* 2016;76:343-8.
10. Williams JC Jr, Al-Awadi H, Muthenini M, et al. Stone Morphology Distinguishes Two Pathways of Idiopathic Calcium Oxalate Stone Pathogenesis. *J Endourol* 2022;36:694-702.
11. Coe FL, Evan A, Worcester E. Kidney stone disease. *J Clin Invest* 2005;115:2598-608.

12. Khan SR. Hyperoxaluria-induced oxidative stress and antioxidants for renal protection. *Urol Res* 2005;33:349-57.
13. Guzel A, Yunusoglu S, Calapoglu M, et al. Protective Effects of Quercetin on Oxidative Stress-Induced Tubular Epithelial Damage in the Experimental Rat Hyperoxaluria Model. *Medicina (Kaunas)* 2021;57:566.
14. Rayman MP. The importance of selenium to human health. *Lancet* 2000;356:233-41.
15. Hadrup N, Ravn-Haren G. Acute human toxicity and mortality after selenium ingestion: A review. *J Trace Elem Med Biol* 2020;58:126435.
16. Wang H, Chen F, Hu A, et al. Harmine loaded Au@MSNs@PEG@Asp6 nano-composites for treatment of spinal metastasis from lung adenocarcinoma by targeting ANXA9 in vivo experiment. *Transl Lung Cancer Res* 2023;12:1062-77.
17. Deng G, Niu K, Zhou F, et al. Treatment of steroid-induced osteonecrosis of the femoral head using porous Se@SiO(2) nanocomposites to suppress reactive oxygen species. *Sci Rep* 2017;7:43914.
18. Zhu Y, Deng G, Ji A, et al. Porous Se@SiO(2) nanospheres treated paraquat-induced acute lung injury by resisting oxidative stress. *Int J Nanomedicine* 2017;12:7143-52.
19. Jia Z, Wang S, Tang J, et al. Does crystal deposition in genetic hypercalciuric rat kidney tissue share similarities with bone formation? *Urology* 2014. doi: 10.1016/j.urology.2013.11.004.
20. Trinchieri A. Epidemiology of urolithiasis. *Arch Ital Urol Androl* 1996;68:203-49.
21. Scales CD Jr, Smith AC, Hanley JM, et al. Prevalence of kidney stones in the United States. *Eur Urol* 2012;62:160-5.
22. Chewcharat A, Curhan G. Trends in the prevalence of kidney stones in the United States from 2007 to 2016. *Urolithiasis* 2021;49:27-39.
23. Zhao Y, Fan Y, Wang M, et al. Kidney stone disease and cardiovascular events: a study on bidirectional causality based on mendelian randomization. *Transl Androl Urol* 2021;10:4344-52.
24. Wang XF, Zhang BH, Lu XQ, et al. Gastrin-releasing peptide receptor gene silencing inhibits the development of the epithelial-mesenchymal transition and formation of a calcium oxalate crystal in renal tubular epithelial cells in mice with kidney stones via the PI3K/Akt signaling pathway. *J Cell Physiol* 2019;234:1567-77.
25. Bird VY, Khan SR. How do stones form? Is unification of theories on stone formation possible? *Arch Esp Urol* 2017;70:12-27.
26. Ye Z, Xia Y, Zhou X, et al. CXCR4 inhibition attenuates calcium oxalate crystal deposition-induced renal fibrosis. *Int Immunopharmacol* 2022;107:108677.
27. Khan SR. Reactive oxygen species, inflammation and calcium oxalate nephrolithiasis. *Transl Androl Urol* 2014;3:256-76.
28. Yifan Z, Luming S, Wei C, et al. Cystine crystal-induced reactive oxygen species associated with NLRP3 inflammasome activation: implications for the pathogenesis of cystine calculi. *Int Urol Nephrol* 2022;54:3097-106.
29. Gerber PA, Rutter GA. The Role of Oxidative Stress and Hypoxia in Pancreatic Beta-Cell Dysfunction in Diabetes Mellitus. *Antioxid Redox Signal* 2017;26:501-18.
30. Scicchitano P, Cortese F, Gesualdo M, et al. The role of endothelial dysfunction and oxidative stress in cerebrovascular diseases. *Free Radic Res* 2019;53:579-95.
31. Chamorro Á, Dirnagl U, Urra X, et al. Neuroprotection in acute stroke: targeting excitotoxicity, oxidative and nitrosative stress, and inflammation. *Lancet Neurol* 2016;15:869-81.
32. Taylor EN, Stampfer MJ, Curhan GC. Diabetes mellitus and the risk of nephrolithiasis. *Kidney Int* 2005;68:1230-5.
33. Alexander RT, Hemmelgarn BR, Wiebe N, et al. Kidney stones and cardiovascular events: a cohort study. *Clin J Am Soc Nephrol* 2014;9:506-12.
34. Enogieru AB, Haylett W, Hiss DC, et al. Rutin as a Potent Antioxidant: Implications for Neurodegenerative Disorders. *Oxid Med Cell Longev* 2018;2018:6241017.
35. Zhang P, Li T, Wu X, et al. Oxidative stress and diabetes: antioxidative strategies. *Front Med* 2020;14:583-600.
36. Zhu J, Wang Q, Li C, et al. Inhibiting inflammation and modulating oxidative stress in oxalate-induced nephrolithiasis with the Nrf2 activator dimethyl fumarate. *Free Radic Biol Med* 2019;134:9-22.
37. Ye QL, Wang DM, Wang X, et al. Sirt1 inhibits kidney stones formation by attenuating calcium oxalate-induced cell injury. *Chem Biol Interact* 2021;347:109605.
38. Li X, Wang Q, Deng G, et al. Porous Se@SiO2 nanospheres attenuate cisplatin-induced acute kidney injury via activation of Sirt1. *Toxicol Appl Pharmacol* 2019;380:114704.
39. Deng G, Chen C, Zhang J, et al. Se@SiO(2) nanocomposites attenuate doxorubicin-induced cardiotoxicity through combatting oxidative damage. *Artif Cells Nanomed Biotechnol* 2018;46:112-21.

40. Khan SR, Joshi S, Wang W, et al. Regulation of macromolecular modulators of urinary stone formation by reactive oxygen species: transcriptional study in an animal model of hyperoxaluria. *Am J Physiol Renal Physiol*

2014;306:F1285-95.

41. Yang Y, Hong S, Wang Q, et al. Exosome-mediated crosstalk between epithelial cells amplifies the cell injury cascade in CaOx stone formation. *J Biol Eng* 2023;17:16.

Cite this article as: Ye C, Zhao L, Miao J, Gong C, Chen Y, Qin S, Tadros NN, Aufderklamm S, Jiang W, Deng G, Ming S. Porous Se@SiO₂ nanocomposites play a potential inhibition role in hyperoxaluria associated kidney stone by exerting antioxidant effects. *Transl Androl Urol* 2024;13(4):526-536. doi: 10.21037/tau-23-511